Journal of Materials Chemistry

Cite this: J. Mater. Chem., 2011, 21, 5604

www.rsc.org/materials

PAPER

Solid state synthesis of $LiFePO_4$ studied by *in situ* high energy X-ray diffraction

Zonghai Chen,*[a] Yang Ren,[b] Yan Qin,[a] Huiming Wu,[a] Shengqian Ma,[ac] Jianguo Ren,[a] Xiangming He,[d] Y.-K. Sun[e] and Khalil Amine*[a]

Received 22nd November 2010, Accepted 13th January 2011
DOI: 10.1039/c0jm04049e

The phase evolution and crystal structure transition of materials during solid-state synthesis of $LiFePO_4$ were investigated by *in situ* high energy X-ray diffraction. It was found that the solid state reaction forming $LiFePO_4$ started at a very low temperature, and $LiFePO_4$ was clearly observed when the reaction temperature was above 173 °C. *In situ* X-ray diffraction data also revealed that several impurities appeared when the reaction temperature was above 400 °C. These impurities were successfully indexed with *ex situ* X-ray diffraction as Li_3PO_4, Fe_2P, and Fe_3P.

Introduction

Research efforts are in progress worldwide to develop reliable, high-performance cathode materials for advanced lithium-ion batteries, paving the way to a secure and sustainable energy future. Among these massive research efforts, there have been reports on low reproducibility of some cathode materials, large discrepancy on cathode performance from group to group, and intense debate on criteria to guide material discovery and design. It is impossible to resolve these issues without a systematic understanding of the structure–property relationship of candidate cathode materials. For instance, $LiFePO_4$ was first reported by Goodenough and coworkers as a potential cathode material for lithium-ion batteries in 1997.[1,2] Because of its low electronic conductivity[3,4] and Li^+ mobility through the $LiFePO_4/FePO_4$ interfaces,[2,3] the major improvement on power capability of $LiFePO_4$ was not reported until recently that extremely high rates could be achieved with $LiFePO_4$ by chemical doping of metal supervalent to Li in nano-structured $LiFePO_4$[5] or off-stoichiometry synthesis to generate a special surface coating.[6] However, the mechanism of the performance improvement is still under debate, and a guideline for successful material design has not been established yet.

[a]*Chemical Sciences and Engineering Division, Argonne National Laboratory, 9700 South Cass Avenue, Lemont, IL, 60439, USA. E-mail: zonghai.chen@anl.gov; amine@anl.gov*
[b]*X-ray Science Division, Advanced Photon Source, Argonne National Laboratory, 9700 South Cass Avenue, Lemont, IL, 60439, USA*
[c]*Department of Chemistry, University of South Florida, Tampa, Florida, 33620, USA*
[d]*Tsing Hua University, Institute of Nuclear Science & New Energy Technology, Beijing, 100084, PR China*
[e]*Department of WCU Energy Engineering, Hanyang University, Seoul, 133-791, South Korea*

It is common practice now to develop nano-structured materials to mitigate the low bulk conductivity of $LiFePO_4$ by reducing the diffusion length of Li ions.[5–8] Furthermore, a conductive carbon coating using various fabrication processes and carbon sources is also widely used to promote the electronic conductivity of olivine materials.[9–12] Besides these incremental improvements, a major improvement was reported by Chiang and coworkers, who improved the electronic conductivity of $LiFePO_4$ by a factor of $\sim 10^8$ by doping metal supervalent to Li^+ site, such as $[Li_{0.99}Nb_{0.01}]FePO_4$.[5] However, this doping mechanism was seriously questioned by subsequent studies from different groups.[3,13,14] Using X-ray diffraction and neutron diffraction data, Nazar *et al.* reported that the supervalent doping of Li^+ site is possible, but offered no evidence connecting the supervalent doping to the dramatic electronic conductivity improvement.[15] Nazar *et al.*[16] studied the surface of carbon-coated $LiFePO_4$ synthesized at 600 °C using Mössbauer and X-ray photoelectron spectroscopy, and observed some impurity components other than simple carbon coating on the $LiFePO_4$ surface. They believed that the impurity was a mixture of Li_3PO_4, FeP, and Fe_2P, and that the iron phosphide coating was the key contributor to the dramatic boost in the electronic conductivity of the $LiFePO_4$ particles.[16] Aiming at understanding the structure–property relationship of $LiFePO_4$, Ceder *et al.* used first principle calculations to predict the Li–Fe–P–O_2 phase diagrams for different synthesis environments,[17] and believed that a Li_3PO_4 coating was the key factor in the performance enhancement.[6] As pointed out by Ceder *et al.*, the solid state reaction for $LiFePO_4$ synthesis is a complicated process that depends on the reducing environment and stoichiometry of the starting materials. Experimental effort to validate these theoretical predictions has not been reported yet.

In this work, *in situ* high energy X-ray diffraction (HEXRD) was used to investigate the phase formation and crystal structure

evolution during solid state synthesis of $LiFePO_4$ using carbothermal reduction process.[18]

Experimental

In situ experiment

The precursor, $FePO_4 \cdot 2H_2O$, was first dehydrated by heating at 500 °C for 6 h in air atmosphere for accurate measurement of iron in the raw material. The anhydrous $FePO_4$ was then mixed with Li_2CO_3 and sugar by ball-milling in water with zirconia balls. This mixing was done for 2 hours with a rotation speed of 450 rpm. The molar ratio of Li_2CO_3 : $FePO_4$: sugar was 0.51 : 1 : 0.1. Sugar was used as (i) the reduction agent to convert Fe(III) to Fe(II) during solid state reaction, and (ii) the precursor of carbon coating on $LiFePO_4$ particles, on which the carbon coating further acts as the reduction agent to partially decompose $LiFePO_4$ into other impurities at a temperature above 400 °C. About 2% excess Li_2CO_3 was added with an initial expectation to compensate for the loss of Li_2O during solid state reaction; this aspect will be discussed later.

After the ball milling, the mixture was dried at 120 °C for 5 hours and pressed into pellets about 2 mm in thickness. Some crystalline water can be there in the sample due to the low drying temperature and direct exposal of samples to the ambient air. The pellet was sandwiched between an alumina can and a platinum cover with holes ($\Phi = 1$ mm) on the centers of both can and cover. The sample was then placed vertically in a programmable furnace with glass windows and Ar was used as the protective gas. The sample was heated up to 600 °C with a heating rate of 2 °C per minute. The *in situ* XRD experiment was carried out at the sector 11 of Advanced Photon Source (APS) of Argonne National Laboratory, the wavelength of X-ray used was pre-set to 0.107805 Å (fixed wavelength for this station). The high energy X-ray source at about 0.1 Å was selected for its excellent penetration capability to detect structural changes on bulk part of the sample. The high flux of X-ray beam at APS is a major advantage to carry out fast experiments at one spectrum per minute. During the course of solid state synthesis, a high energy X-ray hit the sample horizontally (see Fig. 1), and a 2D X-ray detector was used to collect the X-ray diffraction (XRD) profiles using a transmission mode with a speed of one spectrum per minute.

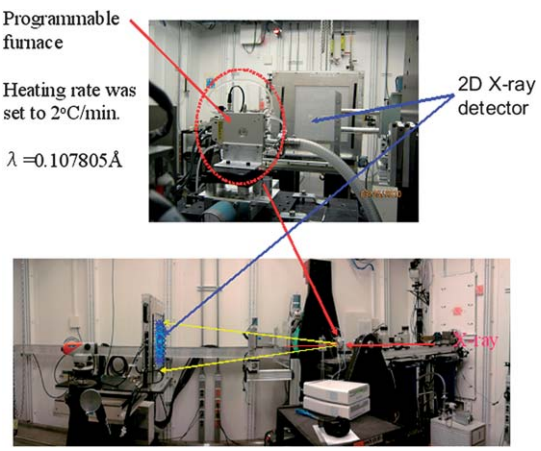

Fig. 1 Images of *in situ* HEXRD experimental setup.

The collected 2D pattern was then integrated into conventional 1D data (intensity *vs.* 2θ) for final data analysis and fitting with GSAS (general structure analysis software).[19] Rietveld refinement using GSAS was carried out to perform (1) background and zero point calibration, (2) X-ray source profile calibration, (3) cell parameter optimization and (4) Li–Fe inter-mixing analysis for $LiFePO_4$.

Ex situ experiment

After the *in situ* experiment, the sample was further heated to 650 °C and sintered for 10 hours to accumulate more impurities. After the sample was cooled to room temperature, the XRD pattern of the sintered sample was collected with the integration time set to one minute, the same as used for the *in situ* experiment. The *ex situ* XRD pattern was then analyzed with GSAS to identify the formula and structures of the impurities.

Results and discussion

Fig. 2a shows the XRD pattern of the mixed starting material before heat treatment. The sample was prepared by simple drying of the wet mixture. The starting materials were not well crystallized, showing broadened peaks. We compared the peak positions and intensities of the XRD pattern against those for each individual component found in the inorganic crystal structure database (ICSD).[20] As shown in Fig. 2b and c, most of the diffraction peaks can be well indexed by $FePO_4$ ($P3_221$, space group # 152) and Li_2CO_3 ($C12/c1$, space group # 15). Fig. 2a also shows four minor peaks (marked by asterisks) that we were not able to index, and they were believed to belong to the sugar added in the mixture, since these peaks disappeared during the solid state synthesis. Fig. 2d shows the peak positions and relative intensities of the expected product, $LiFePO_4$ (*Pnma*, space group # 62). The (200) peak of $LiFePO_4$ at about 1.2° can be used as the characteristic peak to index the existence of $LiFePO_4$. Similarly, $FePO_4$ can be specifically indexed by its strong (100) peak at about 1.41°, and Li_2CO_3 can be indexed using its (110) peak at about 1.48°. Fig. 2a also shows four extra diffraction peaks that are marked by asterisks and that are indexed by sucrose ($C_{12}H_{22}O_{11}$) (Card # 000-024-1977 in the Powder

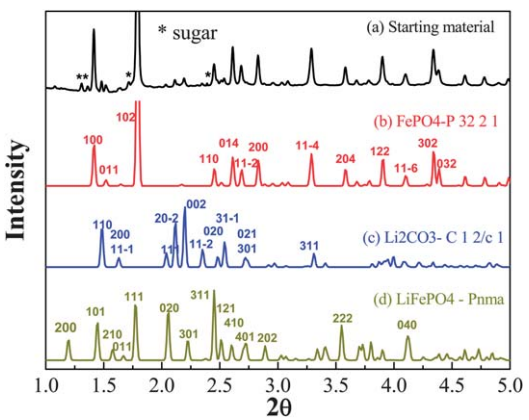

Fig. 2 XRD pattern of the starting material and the simulated XRD pattern of $FePO_4$, Li_2CO_3, and $LiFePO_4$ determined from the inorganic crystal structure database.

Diffraction Files of the International Center for Diffraction Data).

Fig. 3 shows the contour plot of the *in situ* HEXRD patterns during the solid state synthesis of $LiFePO_4$ with the temperature increasing from 32 °C to 600 °C at a heating rate of 2 °C per minute. All peaks shifted slightly to a lower angle with the increase of the reaction temperature. This shift is primarily caused by the thermal expansion of the crystals and is not conclusive evidence for the phase transformation. The first clear indication of a phase change occurred during the initial heating up to 200 °C. Because the diffraction intensity from the sample is very low in the temperature range between 125 °C and 200 °C, detailed diffraction patterns at various temperatures from 32 °C to 205 °C are illustrated separately in Fig. 4. This figure clearly shows that the (200) peak of $LiFePO_4$ at about 1.2° appeared when the temperature was above 164°, and that the (102) peak of $FePO_4$ at 1.41° disappeared at about 134 °C. However, the (100) peak of Li_2CO_3 at 1.48° steadily decreased with the reaction temperature and did not completely disappear until 205 °C. A possible explanation of this low diffraction intensity zone is as follows. The hydrated iron phosphate ($FePO_4 \cdot xH_2O$) started to lose its crystalline water as the temperature increased and formed nano-clusters of dehydrated $FePO_4$, leading to a rapid decrease of the peak intensity. After the normalizing the intensity of (200) peak, no obvious peak broadening was observed from 32 °C to 164 °C. Therefore, it was believed that $FePO_4$ was formed in amorphous state. When the temperature was above 164 °C, solid state reaction among amorphous $FePO_4$, Li_2CO_3, and sugar started led to gradual consumption of Li_2CO_3 and accumulation of $LiFePO_4$.

To confirm our speculation that the solid state reaction can occur at a temperature as low as 164 °C, we performed thermal gravimetric analysis (TGA) on a fresh sample in an Ar environment with a heating rate of 1 °C per minute. The weight loss and derivative weight loss of the sample are plotted in Fig. 5 as a function of the sample temperature. The top panel of Fig. 5 shows a slow but accelerated weight loss during the initial heating, which can be related to the dehydration of starting material as proposed above to explain the HEXRD patterns. After that, a sharp major reaction was observed at about 173 °C, leading to about 5% weight loss in 10 minutes. Combining the

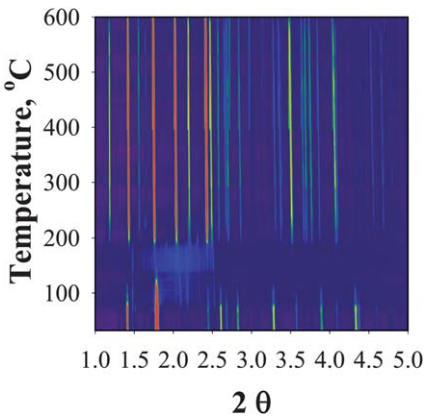

Fig. 3 Contour plot of XRD patterns collected during the solid state synthesis.

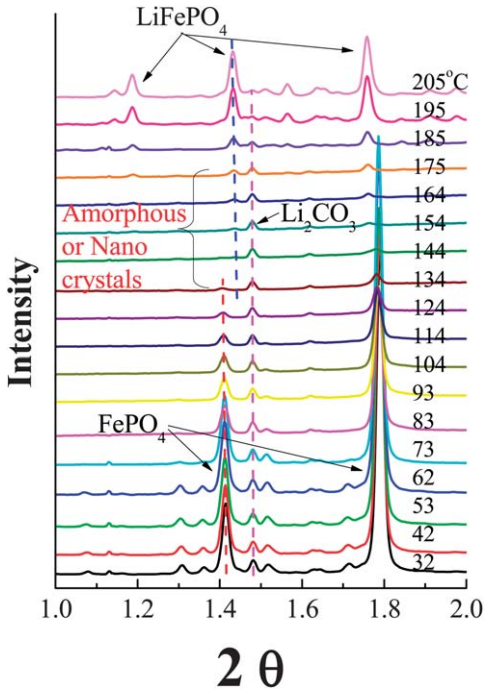

Fig. 4 XRD pattern of the material during the initial stage between room temperature and 200 °C, showing the progress of the solid state reaction.

XRD patterns (Fig. 4) and the TGA data (Fig. 5), we can draw the conclusion that the reaction at this low temperature was related to the solid state reaction that formed $LiFePO_4$, and that the major weight loss was due to the loss of CO_2 from Li_2CO_3 and oxidation of sugar to balance the reduction of Fe(III) to Fe(II). We believe that the liquid sugar, whose melting point is about 155 °C, facilitated the diffusion of Li(I) into the $FePO_4$ nano-clusters, so that the solid state reaction occurred at such low temperature.

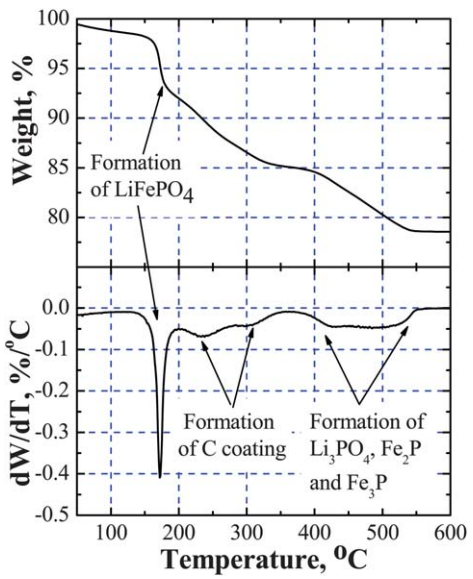

Fig. 5 TGA analysis of starting material in Ar with a heating rate of 1 °C min^{-1}.

The TGA data in Fig. 5 show a continuous multiple-step reaction from initial heating up to about 580 °C, after which the sample weight stabilized. The weight loss curve of Fig. 5 shows poor resolution between reactions, and hence the derivative curve *vs.* sample temperature was calculated and is shown in the bottom panel. Besides the solid state reaction to form $LiFePO_4$ that peaks at 173 °C, four minor broad peaks can be seen at 237 °C, 306 °C, 431 °C, and 503 °C. As later confirmed by *ex situ* XRD, the peaks at above 400 °C are associated with the reduction of $LiFePO_4$ by carbon and generate a mixture impurity of Li_3PO_4, Fe_2P, and Fe_3P. In the scope of this work, we were not able to collect conclusive evidence to index the carbonization reaction of sugar during the synthesis. The carbonization of sugar may have occurred in the temperature window between 200 °C and 350 °C. More experimental study in this temperature window needs to be conducted to confirm our speculation.

Fig. 6A shows the XRD pattern collected when the sampled was heated up to 299 °C along with the simulated XRD pattern for $LiFePO_4$. An excellent fit was obtained by using the cell parameters shown in Fig. 6A, with very small fitting residue. The XRD pattern and its fit clearly indicate the formation of pure $LiFePO_4$ at low temperature. Rietveld refinement was carried out on XRD patterns collected in the temperature window from 200 °C to 600 °C (the XRD pattern not shown). The XRD pattern collected at 201 °C shows some minor peaks that cannot be fit by the simulated XRD pattern for $LiFePO_4$. These peaks represent some residues from the starting materials since the solid state reaction was not fully complete yet. Other XRD patterns collected from 251 °C to 501 °C were all well fitted, and their corresponding lattice parameters are shown in Fig. 6B. All three parameters showed a strong linear correlation with each other, and all increased linearly with the temperature. These trends are believed to be caused by the thermal expansion of the lattice, leading to the shift of the diffraction peaks to lower angles (see Fig. 2).

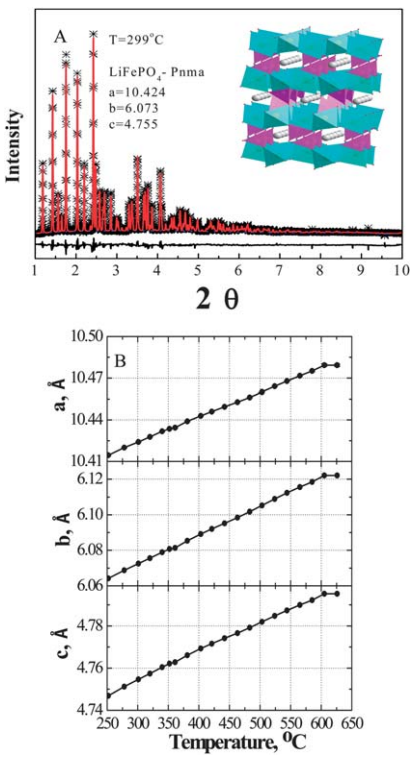

Fig. 6 (A) XRD pattern and fit to simulated pattern for the material heated up to 299 °C, showing the emergence of pure and single-phase $LiFePO_4$. (B) Cell parameters of obtained $LiFePO_4$ as function of temperature.

It was also found that the fitting residues increased steadily with the temperature above 400 °C, and most of the residue peaks are centered in a small 2θ range between 2.0° and 3.0°. Hence, a contour plot from the XRD patterns was prepared to show the diffraction peaks in this narrow 2θ range. As shown in Fig. 7, several peaks appeared when the temperature was above 400 °C, suggesting emergence of new impurities when synthesizing $LiFePO_4$ at high temperature. In addition, these weak peaks all appeared as left shoulders of major diffraction peaks of $LiFePO_4$, and the impurities also showed less thermal expansion than $LiFePO_4$. As a consequence, these weak peaks finally merged into the strong peaks of $LiFePO_4$ as the temperature increased, making them difficult to be observed. Our interest is to accurately index the formula and structure of the impurities. Therefore, the sample after the *in situ* experiment was further heated up to 650 °C and sintered at 650 °C for 10 hours to accumulate more impurities to ease the structural analysis. The *ex situ* XRD pattern was collected at room temperature to obtain better resolution between $LiFePO_4$ and the impurities. Fig. 8 shows the *ex situ* XRD pattern as well as its fit using four species: Li_3PO_4 (*Pmnb*), Fe_2P ($P\bar{6}2m$), Fe_3P ($I\bar{4}$), and $LiFePO_4$ (*Pnma*). The experimental and simulated patterns agreed well, as shown in Fig. 8a. The XRD pattern shows no evidence of the FeP impurity that was proposed by Nazar *et al.*[16]

Fig. 9 shows a simplified Li–Fe–P ternary phase diagram to help understand the results from the *ex situ* XRD pattern.[17] In the starting material, 2% excess Li_2CO_3 was added to compensate for the potential loss of Li_2O during the high temperature reaction and to obtain stoichiometric $LiFePO_4$, shown at the center of the phase diagram (Fig. 9). Fig. 8 shows that the extra impurities detected are Fe_2P, Fe_3P, and Li_3PO_4, which are also labeled in Fig. 9. Also note in Fig. 9 that the composition of $LiFePO_4$ is sitting right outside the triangle formed by Fe_2P,

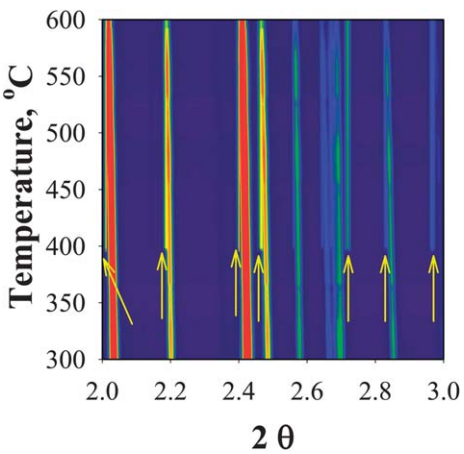

Fig. 7 Contour plot of XRD patterns showing the emergence of impurities at above 400 °C.

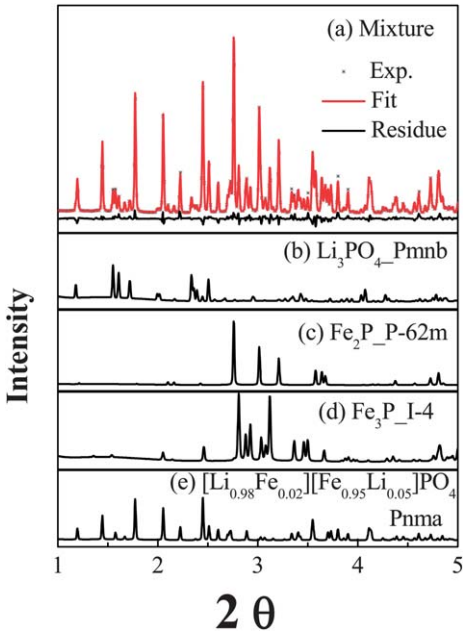

Fig. 8 *Ex situ* XRD pattern and fit to simulated pattern for the sample baked at 650 °C for 10 hours. The XRD pattern was collected at room temperature.

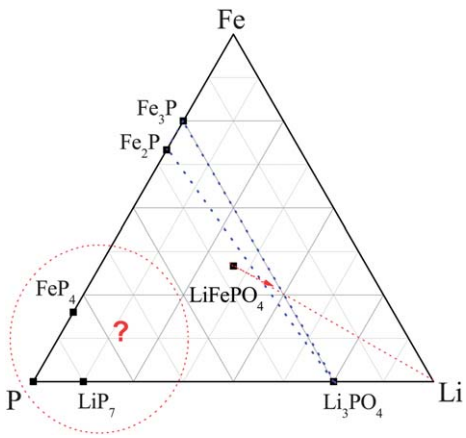

Fig. 9 Simplified phase Li–Fe–P diagram showing possible missed component in the XRD patterns.

Fe_3P, and Li_3PO_4. This suggests that some species must be missing from the phase diagram. A possible explanation is that some species like volatile P_4[16] or other P-abundant amorphous phase was not detected by the XRD pattern. Alternatively, the excess Li_2CO_3 added might actually not have vaporized, but participated in the formation of the impurities and moved the stoichiometry of the starting material into the triangle. This off-stoichiometry route has been used by Ceder *et al.* to synthesize Li_3PO_4-coated $LiFePO_4$ by adding less Fe- and P-based raw materials.[6]

Others have reported that these impurities are crucial to boost the electrochemical performance of $LiFePO_4$ cathode material.[6,16] However, the exact content of the impurities reported here is different from that reported by others.[6,16] The common ground of this work and previous reports is that the obtained impurity is generally a mixture of several species, and the specific effect of each component on the electrochemical performance has not been conclusively quantified yet. It is of great importance to selectively synthesize $LiFePO_4$ cathode materials with different impurity contents to isolate and quantify the impact of each component, including the carbon coating.[21] As mentioned above, it is difficult to carry out quantitative analysis on the impurities using *in situ* XRD data, and more research effort is needed to carry out *ex situ* experiments and to quantitatively establish the electrochemical performance and the evolution of impurities, as well as the carbon coating.

Conclusion

In situ high energy X-ray diffraction was deployed to study the phase evolution during the solid state synthesis of $LiFePO_4$. The solid state reaction occurred at a temperature as low as 173 °C, and impurities including Li_3PO_4, Fe_2P, and Fe_3P emerged when the synthesizing temperature was above 400 °C. We believe that this *in situ* technique is a powerful tool for studying the structure–property relationship of electrode materials and can be easily applied to other classes of materials.

Acknowledgements

Research at Argonne National Laboratory was funded by US Department of Energy, FreedomCAR and Vehicle Technologies Office. Argonne National Laboratory is operated for the US Department of Energy by UChicago Argonne, LLC, under contract DE-AC02-06CH11357. This work was also supported by the National Research Foundation of Korea Grant funded by the Korean Government (MEST) (NRF-2009-C1AAA001-0093307).

References

1 A. K. Padhi, K. S. Nanjundaswamy, C. Masquelier, S. Okada and J. B. Goodenough, Effect of structure on the Fe3+/Fe2+ redox couple in iron phosphates, *J. Electrochem. Soc.*, 1997, **144**(5), 1609–1613.
2 A. K. Padhi, K. S. Nanjundaswamy and J. B. Goodenough, Phospho-olivines as positive-electrode materials for rechargeable lithium batteries, *J. Electrochem. Soc.*, 1997, **144**(4), 1188–1194.
3 P. S. Herle, B. Ellis, N. Coombs and L. F. Nazar, Nano-network electronic conduction in iron and nickel olivine phosphates, *Nat. Mater.*, 2004, **3**(3), 147–152.
4 C. Delacourt, L. Laffont, R. Bouchet, C. Wurm, J. B. Leriche, M. Morcrette, J. M. Tarascon and C. Masquelier, Toward understanding of electrical limitations (electronic, ionic) in LiMPO4 (M = Fe, Mn) electrode materials, *J. Electrochem. Soc.*, 2005, **152**(5), A913–A921.
5 S. Y. Chung, J. T. Bloking and Y. M. Chiang, Electronically conductive phospho-olivines as lithium storage electrodes, *Nat. Mater.*, 2002, **1**(2), 123–128.
6 B. Kang and G. Ceder, Battery materials for ultrafast charging and discharging, *Nature*, 2009, **458**(7235), 190–193.
7 B. Ellis, P. S. Herle, Y. H. Rho, L. F. Nazar, R. Dunlap, L. K. Perry and D. H. Ryan, Nanostructured materials for lithium-ion batteries: surface conductivity *vs.* bulk ion/electron transport, *Faraday Discuss.*, 2007, **134**, 119–141.
8 C. Delacourt, P. Poizot, S. Levasseur and C. Masquelier, Size effects on carbon-free LiFePO4 powders, *Electrochem. Solid-State Lett.*, 2006, **9**(7), A352–A355.
9 Z. H. Chen and J. R. Dahn, Reducing carbon in LiFePO4/C composite electrodes to maximize specific energy, volumetric energy, and tap density, *J. Electrochem. Soc.*, 2002, **149**(9), A1184–A1189.

10 H. Goktepe, H. Sahan, F. Kilic and S. Patat, Improved of cathode performance of LiFePO4/C composite using different carboxylic acids as carbon sources for lithium-ion batteries, *Ionics*, 2010, **16**(3), 203–208.
11 I. Belharouak, C. Johnson and K. Amine, Synthesis and electrochemical analysis of vapor-deposited carbon-coated LiFePO4, *Electrochem. Commun.*, 2005, **7**(10), 983–988.
12 S. W. Oh, S. T. Myung, S. M. Oh, C. S. Yoon, K. Amine and Y. K. Sun, Polyvinylpyrrolidone-assisted synthesis of microscale C-LiFePO4 with high tap density as positive electrode materials for lithium batteries, *Electrochim. Acta*, 2010, **55**(3), 1193–1199.
13 C. Delacourt, C. Wurm, L. Laffont, J. B. Leriche and C. Masquelier, Electrochemical and electrical properties of Nb- and/or C-containing LiFePO4 composites, *Solid State Ionics*, 2006, **177**(3–4), 333–341.
14 M. S. Islam, D. J. Driscoll, C. A. J. Fisher and P. R. Slater, Atomic-scale investigation of defects, dopants, and lithium transport in the LiFePO4 olivine-type battery material, *Chem. Mater.*, 2005, **17**(20), 5085–5092.
15 M. Wagemaker, B. L. Ellis, D. Luetzenkirchen-Hecht, F. M. Mulder and L. F. Nazar, Proof of supervalent doping in olivine LiFePO4, *Chem. Mater.*, 2008, **20**(20), 6313–6315.
16 Y. H. Rho, L. F. Nazar, L. Perry and D. Ryan, Surface chemistry of LiFePO4 studied by mossbauer and X-ray photoelectron spectroscopy and its effect on electrochemical properties, *J. Electrochem. Soc.*, 2007, **154**(4), A283–A289.
17 S. P. Ong, L. Wang, B. Kang and G. Ceder, Li–Fe–P–O–2 phase diagram from first principles calculations, *Chem. Mater.*, 2008, **20**(5), 1798–1807.
18 B. Q. Zhu, X. H. Li, Z. X. Wang and H. J. Guo, Novel synthesis of LiFePO4 by aqueous precipitation and carbothermal reduction, *Mater. Chem. Phys.*, 2006, **98**(2–3), 373–376.
19 A. C. Larson, R. B. V. Dreeele, *General Structure Analysis System (GSAS)*, Los Alamos national Laboratory, Report LAUR 86-748, 2004.
20 http://icsd.fiz-karlsruhe.de/icsd/.
21 C. M. Julien, K. Zaghib, A. Mauger, M. Massot, A. Ait-Salah, M. Selmane and F. Gendron, Characterization of the carbon coating onto LiFePO4 particles used in lithium batteries, *J. Appl. Phys.*, 2006, **100**(6), 63511–63517.